THE **EUROPEAN**
PHYSICAL JOURNAL A

Regular Article – Experimental Physics

Reduction of deuterium content in carbon targets for ^{12}C $+$ ^{12}C reaction studies of astrophysical interest

L. Morales-Gallegos[1,2], M. Aliotta[1,3,a], C.G. Bruno[1], R. Buompane[3,2], T. Davinson[1], M. De Cesare[4,2], A. Di Leva[5,2], A. D'Onofrio[3,2], J.G. Duarte[3,2], L.R. Gasques[6,3,2], L. Gialanella[3,2,b], G. Imbriani[5,2], G. Porzio[3], D. Rapagnani[7,8], M. Romoli[2], D. Schürmann[3,2], F. Terrasi[3,2], and L.Y. Zhang[9,1]

[1] SUPA, School of Physics and Astronomy, University of Edinburgh, Edinburgh, UK
[2] INFN, Sezione di Napoli, Napoli, Italy
[3] Dipartimento di Matematica e Fisica, Università degli Studi della Campania "Luigi Vanvitelli", Caserta, Italy
[4] Centro Italiano di Ricerche Aerospaziali, Capua, Italy
[5] Dipartimento di Fisica "E. Pancini", Università degli Studi di Napoli "Federico II", Napoli, Italy
[6] Departamento de Física Nuclear, Instituto de Física da Universidade de São Paulo, São Paulo, Brazil
[7] Dipartimento di Fisica e Geologia, Università degli Studi di Perugia, Perugia, Italy
[8] INFN, Sezione di Perugia, Perugia, Italy
[9] National Astronomical Observatories, Chinese Academy of Sciences, Lanzhou, China

Abstract. The ^{12}C(^{12}C, p)^{23}Na and ^{12}C(^{12}C, α)^{20}Ne fusion reactions are among the most important in stellar evolution since they determine the destiny of massive ($M \simeq 8$–$10 \, M_\odot$) stars. However, experimental low-energy investigations of such reactions are significantly hampered by ubiquitous natural hydrogen and deuterium contaminants in the carbon targets. The associated beam-induced background completely masks the reaction products of interest thus preventing cross-section measurements at the relevant energies of astrophysical interest, $E_{\rm cm} < 2 \, {\rm MeV}$. In this work, we report about an investigation aimed at assessing possible deuterium reductions on both natural graphite and Highly Ordered Pyrolytic Graphite targets as a function of target temperature. Our results indicate that reductions up to about 80% can be attained on both targets in the temperature range investigated, $T \simeq 200$–$1200\,^\circ{\rm C}$. A further reduction by a factor of 2.5 in absolute deuterium content is observed when the scattering chamber is surrounded by a dry nitrogen atmosphere so as to minimise light-particles uptake within the chamber rest gas (and thus on target) through air leaks. The results from this study will inform the choice of optimal experimental conditions and procedures for improved measurements of the ^{12}C $+$ ^{12}C reactions cross-sections at the low energies of astrophysical interest.

1 Introduction

The fusion of two ^{12}C nuclei in stars, referred to as carbon burning, plays a key role in the evolution of massive stars and determines whether these will end up as white dwarfs or as core-collapse supernovae [1,2]. Carbon burning proceeds mainly through two channels: ^{12}C(^{12}C, p)^{23}Na and ^{12}C(^{12}C, α)^{20}Ne. Direct measurements of both reactions have been performed over a wide range of energies, using either particle spectroscopy [3–5], γ-ray measurements [6–13] or a combination of both techniques [14,15]. Yet, the energy of interest for astrophysical purposes ($E_{\rm cm} <$ 2 MeV) has never been reached experimentally and stellar models have to rely on extrapolations of cross-section data taken at higher energies. Unfortunately, a reliable extrapolation is complicated by the presence of resonances, the nature of which is still a matter of debate [16,17], that are likely to persist at low energies. As a result, current calculations of the non-resonant astrophysical S-factor differ by up to three orders of magnitude in the region below 2.5 MeV. Thus, despite many decades of experimental effort one is still far from the precision ($\approx 10\%$) required to firmly constrain astrophysical models.

A key limitation to low-energy measurements of the ^{12}C $+$ ^{12}C reactions arises from light species contaminations, mostly ^{1}H and ^{2}H, in the carbon targets. Because of the reduced Coulomb barrier, the probability of inducing

[a] e-mail: m.aliotta@ed.ac.uk
[b] e-mail: lucio.gialanella@na.infn.it

a ^{12}C + ^{1,2}H reaction in the target is orders of magnitude higher than the cross-sections of interest and thus even traces of contaminants pose serious challenges to the experimentalists, preventing reliable measurements at energies of astrophysical interest.

Previous studies showed that ^{1,2}H contamination can be reduced by heating the target either through resistive heating of carbon foils (9–88 μg/cm^2) supported by a tantalum backing [7] up to 1800 °C [7] or by beam-power deposition on 1 mm thick graphite targets to 400 °C (for 6–8 hours) [11] and to 700 °C [13]. While a reduction in H contamination was found in all cases, resulting in cleaner spectra at low energies, no systematic investigation was carried out to quantify such a reduction or to assess the best operating conditions for low-energy measurements of the carbon fusion cross-sections.

In this paper, we report on the results of a quantitative study to asses depletion of hydrogen and deuterium impurities of carbon targets *in situ* to avoid unnecessary air exposures (see for example [18]) by means of diffusion at high temperature, as originally suggested in [13]. Measurements conducted under controlled experimental conditions on natural graphite (NG) and Highly Ordered Pyrolytic Graphite (HOPG) targets of different purity show that deuterium (and hydrogen) content can be reduced by up to about 70–85% for HOPG and NG targets at target temperatures above 1000 °C. A further reduction by a factor of about 2.5 is attained when enclosing the scattering chamber in a dry nitrogen atmosphere to minimise air leaks into the rest gas within the chamber.

2 Experimental setup

2.1 CIRCE

The experimental work was carried out at the Centre for Isotopic Research on the Cultural and Environmental heritage (CIRCE) of the Università della Campania "Luigi Vanvitelli", Caserta (Italy). The facility consists of a 3 MV Pelletron tandem accelerator capable of delivering high intensities (up to 50 μA on target) ^{12}C beams with good energy resolution (about 5 keV for an 8 MeV beam). A description of the accelerator and beam properties can be found in [19].

2.2 Scattering chamber

The experimental setup consisted of a large scattering chamber housing a purpose-built detection array (sect. 2.3) and a water-cooled target ladder able to accommodate two targets and two collimators (3 and 6 mm in diameter) for beam focussing purposes. A 3D-printed sphere coated with conductive paint surrounded the target and was kept at −300 V for electron suppression, so as to grant a correct beam-current reading directly on target. Squared openings (25 × 25 mm^2 each, with gold-coated tungsten wire grids) on the sphere allowed for the passage of the beam and the particles to be detected. The pressure in the
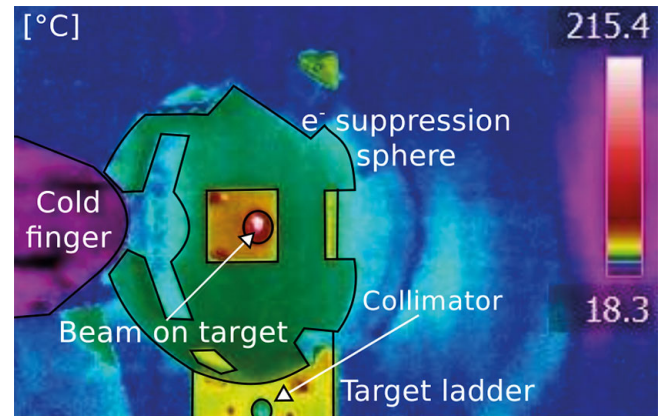
Fig. 1. Tone coded image of the HOPG target taken with the thermo-camera under beam bombardment with a ^{12}C^{3+} beam at laboratory energy $E = 8$ MeV. Contour lines have been added for clarity. Note that the temperature scale shown on the right side is only correct for carbon due to the emissivity value setted on the camera.

chamber was maintained below 5×10^{-7} mbar by means of an oil-free turbo and scroll pump system, in combination with a cold finger pipe protruding from the beam line to 5 cm from the target and maintained at LN$_2$ temperature.

Both HOPG and NG targets were 1 mm thick, had a diameter of 10 mm and were mounted on the water-cooled target ladder. The target temperature during beam bombardment was continuously monitored with a calibrated[1] thermo-camera (FLIR SC325, accuracy ±2% of reading [20]) placed outside the scattering chamber and facing the target through a Ge window[2]. The thermo-camera was modified by the producer so as to extend its sensitivity range up to $T = 1200$ °C. The target temperature at the beam spot was recorded (using the thermo-camera software) as a function of beam current on target for further offline analysis. The target temperature could be changed either by regulating the cooling water flux or by changing the beam current on target. Figure 1 shows a thermal image of the target taken under beam bombardment.

A quadrupole mass spectrometer (QMS, Pfeiffer Prisma 200) mounted on one of the chamber's ports was used to continuously monitor the rest gas in the chamber. In order to minimise contamination of the targets from light-mass species (mostly hydrogen and deuterium) present in the air, the entire chamber was enclosed by a sealed plexiglass structure which could be flooded with dry nitrogen continuously flushed at a slightly higher pressure than atmospheric (hereafter, "aquarium") or left in air. This allowed us to investigate the influence of the nitrogen atmosphere on the composition of the rest gas in the

---

[1] Calibration certificate No. SED04024 by FLIR.

[2] Normal glass is opaque to infrared radiation, whereas the Ge window is transparent to the wavelengths (7.5–13 μm) to which the thermo-camera is sensitive. The attenuation induced by the Ge window is well known and duly taken into account during data analysis.
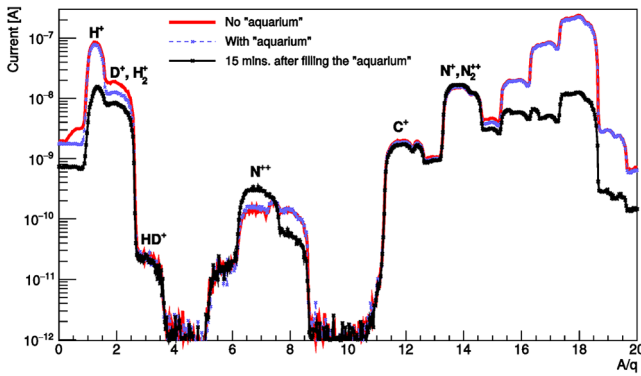
Fig. 2. Overlay of rest-gas composition spectra as a function of mass-to-charge-state ratio $[A/q]$ as measured by the Quadrupole Mass Spectrometer. A reduction in hydrogen and deuterium content is obtained soon after enclosing the scattering chamber in a nitrogen atmosphere ("aquarium").
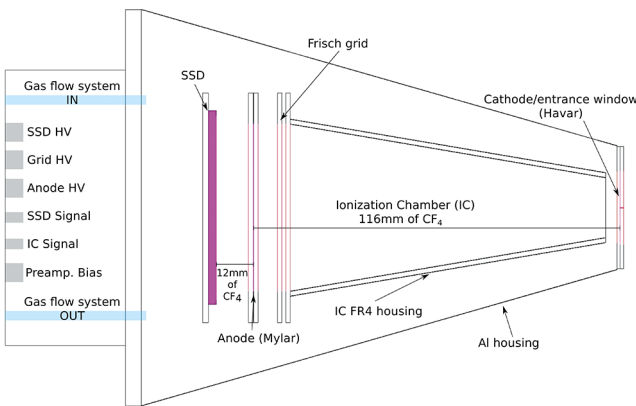

Fig. 3. Schematic view of a GASTLY detector module. Each module consists of an ionisation chamber (ΔE stage) and a large area silicon (strip) detector (E stage). Further details can be found in [21].

scattering chamber. Typical pressure-normalised spectra of rest-gas composition with and without the aquarium are shown in fig. 2. A stable reduction in hydrogen and deuterium in the rest gas by a factor of about 4.5 and 2.5, respectively, was obtained already after 15 minutes from filling the nitrogen aquarium.

2.3 Detectors

A two-stage detection array GASTLY (GAs Silicon Two-Layer sYstem) was specifically designed to detect low-energy light charged-particles and to fulfil the requirements for the ^{12}C + ^{12}C reaction cross-section measurements. The array can accommodate up to eight ΔE-E modules, each comprising an ionisation chamber (IC) and a large area silicon strip detector (SSD). Further details on the full detector array and its commissioning are reported in [21]. Briefly, each module consists in an aluminium pyramidal structure with square base, hosting the IC (ΔE stage) and the SSD (E stage) detector, as shown schematically in fig. 3.
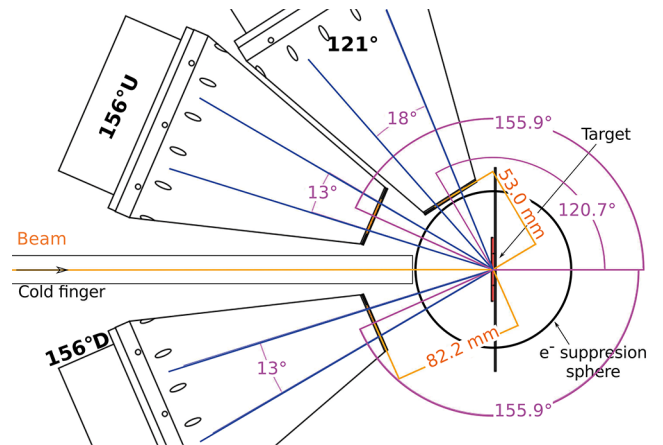
Fig. 4. Side view of the experimental chamber, showing three of the four GASTLY modules used for the present experiment. The fourth module was placed on the horizontal plane at an angle of 143.2° from the beam axis. Also sketched are the target, the 3D-printed sphere for electron beam suppression, and the LN$_2$-cooled copper cold finger (see text for details).

The IC is equipped with an entrance Havar window ($23 \times 23\,\mathrm{mm}^2$ large and $2.6\,\mu\mathrm{m}$ thick) acting as a cathode; an aluminised Mylar foil ($52.5 \times 52.5\,\mathrm{mm}^2$, $1.6\,\mu\mathrm{m}$ thick, metallised with $50\,\mu\mathrm{g/cm}^2$) acting as an anode and placed $116\,\mathrm{mm}$ behind the Havar window; and a Frisch grid, consisting of a mesh of gold-coated tungsten wires ($20\,\mu\mathrm{m}$ diameter). The IC was operated with CF$_4$ maintained at constant pressure of $50\,\mathrm{mbar}$ (within $\pm 0.05\,\mathrm{mbar}$) by means of an automatic system [21].

The second stage of each GASTLY module consists of a large ($58.0 \times 58.0\,\mathrm{mm}^2$ active area, $300 \pm 15\,\mu\mathrm{m}$ thick) silicon strip detector[3] by CANBERRA Ltd. (mod. PF-16CT-58*58-300EB/D4) [22].

For the present study, only four ΔE-E modules were used: three were placed in the vertical plane at angles[4] of 120.7° and 155.9° to the beam axis (hereafter, D121, D156U and D156D, respectively) and one on the horizontal plane at an angle 143.2° to the beam axis (hereafter, D143). The choice of these positions was dictated by the need to guarantee unhindered viewing of the target by the thermo-camera. Detectors D121 and D143 were placed at a (silicon-to-target) distance of 181 mm, subtending a solid angle of 80 msr. Because of mechanical constraints, both D156U and D156D detectors had to be placed at an overall distance of 201 mm, thus subtending a nominal solid angle of 64 msr, which was further reduced to 40 msr owing to a partial shadowing from the IC. See [23] for further details. A (partial) schematic view of the setup is shown in fig. 4.

---

[3] Note that for the present study the silicon detector was used as a single pad, *i.e.*, without making use of its segmentation.

[4] All angles reported here are in the laboratory frame of reference. Their values differ slightly from the nominal ones in [21] due to a 2 mm upstream shift of the target when mounted on the target holder.

3 Beam-induced background considerations

The main aim of the present study was to investigate how contaminant hydrogen and deuterium concentrations in HOPG and NG targets vary as a function of target temperature through intense ^{12}C beam bombardment. This study is relevant when trying to assess beam-induced background in ^{12}C(^{12}C, p)^{23}Na ($Q = 2.241$ MeV) cross section measurements. Six different sources of beam-induced background are possible in principle. Three can be identified as "primary" processes[5], namely: i) p(^{12}C, p)^{12}C, ii) d(^{12}C, d)^{12}C elastic scattering; and iii) d(^{12}C, p)^{13}C transfer reaction ($Q = 2.722$ MeV). Note that the p(^{12}C, d)^{11}C channel ($Q = -16.497$ MeV) remains closed at all energies investigated here. Because of inverse kinematics conditions, only protons from the d(^{12}C, p)^{13}C transfer reaction (case iii)) can be detected at backward angles[6].

Three other processes can be identified as "secondary", as they are initiated by either proton and deuteron contaminants in the target scattered at forward angles by the ^{12}C beam. Their interaction with a further ^{12}C nucleus in the target could then give rise to "secondary" protons through either iv) ^{12}C(p, p)^{12}C and v) ^{12}C(d, d)^{12}C scattering or through a "secondary" vi) ^{12}C(d, p)^{13}C transfer reaction (this latter is sometimes referred to as "two-step" process [24]). Once again, the ^{12}C(p, d)^{11}C remains a closed channel.

For the experimental conditions of our study (sect. 2), protons and deuterons from secondary elastic scattering (cases iv) and v), respectively) are either stopped in the ΔE detector or emerge from it with very little energy and thus remain well outside the region of interest of protons from the ^{12}C(^{12}C, p)^{23}Na reaction. Thus, only secondary protons from the ^{12}C(d, p)^{13}C reaction (case vi)) are of concern as a source of beam-induced background in the proton spectrum.

In summary, for the present investigation, only deuterium impurities in the target give rise to any background protons, through either the primary or secondary reaction d(^{12}C, p)^{13}C and ^{12}C(d, p)^{13}C, respectively.

As discussed in [24], the probability for the ^{12}C(d, p)^{13}C secondary fusion reaction (intrinsically low) is only appreciable for scattered deuteron energies near the resonant value $E_d = 1.2$ MeV. As a result, the position of these secondary protons in the ΔE-E matrix remains essentially unchanged regardless of the ^{12}C beam energy. Eventually, for ^{12}C-beam energies $E_{lab} < 2$ MeV, the energy of scattered deuterons becomes insufficient to excite the resonance and the secondary proton yield decreases drastically (see [24] for further details).

Previous measurements [24] on targets of different nominal purity have shown a positive correlation between deuterium concentration and the yield of secondary pro-

tons, Y_s, from the ^{12}C(d, p)^{13}C process. A measurement of Y_s as a function of ^{12}C-beam energy provided an empirical relationship [24] to estimate and correct for the background induced by the secondary protons. Such a correction becomes critical for measurements of the astrophysical ^{12}C(^{12}C, p)^{23}Na reaction at beam energies $E_{lab} < 5$ MeV, where the measured yield is essentially dominated by secondary protons background [24].

Here, we focus instead on assessing deuterium concentration changes specifically due to the target temperature effects. Since deuterium concentrations may vary from target to target (even with the same nominal purity) and as a result of target exposure (through beam-induced erosion, diffusion, and/or rest gas deposition), constant and *in situ* monitoring of deuterium content must be achieved during measurements. Primary protons produced by the d(^{12}C, p)^{13}C reaction provide a direct way to quantify the level of deuterium contamination *in situ*. In the following, the yield of primary protons, referred to as $Y_p(d)$, is taken as a proxy for the deuterium content in the target.

4 Experimental procedures

4.1 Data taking

Both NG and HOPG targets were bombarded with a ^{12}C^{3+} beam at an energy $E = 8$ MeV and intensities between 10 and 50 μA. The choice of beam energy was dictated by a compromise between high statistics and sufficient separation between proton peaks from the ^{12}C fusion reactions and protons from beam-induced background on hydrogen and deuterium contaminants.

The beam spot on target was visually monitored with the thermo-camera and its diameter found to be typically less than 2.5 mm. As the targets were sufficiently thick ($\simeq 1$ mm) to fully stop the beam, the deposited power led to an increase in target temperature up to 1100 °C, depending on beam current. The target temperature at the beam spot position was continuously monitored and its value recorded for further offline analysis together with the value of the beam current on target. For some runs, the target temperature was kept constant at a desired value by regulating the flux of water in the water-cooling circuit. For other runs, it was left to vary with beam current, and thus with power deposited.

Data were taken under the following conditions: 1) HOPG target without aquarium: here the target temperature decreased from 1100 °C to 200 °C; 2) and 3) HOPG targets with aquarium at constant target temperature of about 900 °C and 1000 °C, respectively; and 4) NG target with aquarium: in this run the target temperature increased from 400 °C to 800 °C. These conditions were chosen as a representative sample of possible combinations within the available beam time.

4.2 Data analysis

Sample proton spectra acquired on NG targets and with the scattering chamber maintained in a nitrogen atmo-

---

[5] Here, we are adopting the standard notation T(b,e)R to indicate the beam (b), target (T), ejectile (e) and recoil (R) nuclei.

[6] Emission of protons from i) and ii) is kinematically impossible at backward angles.
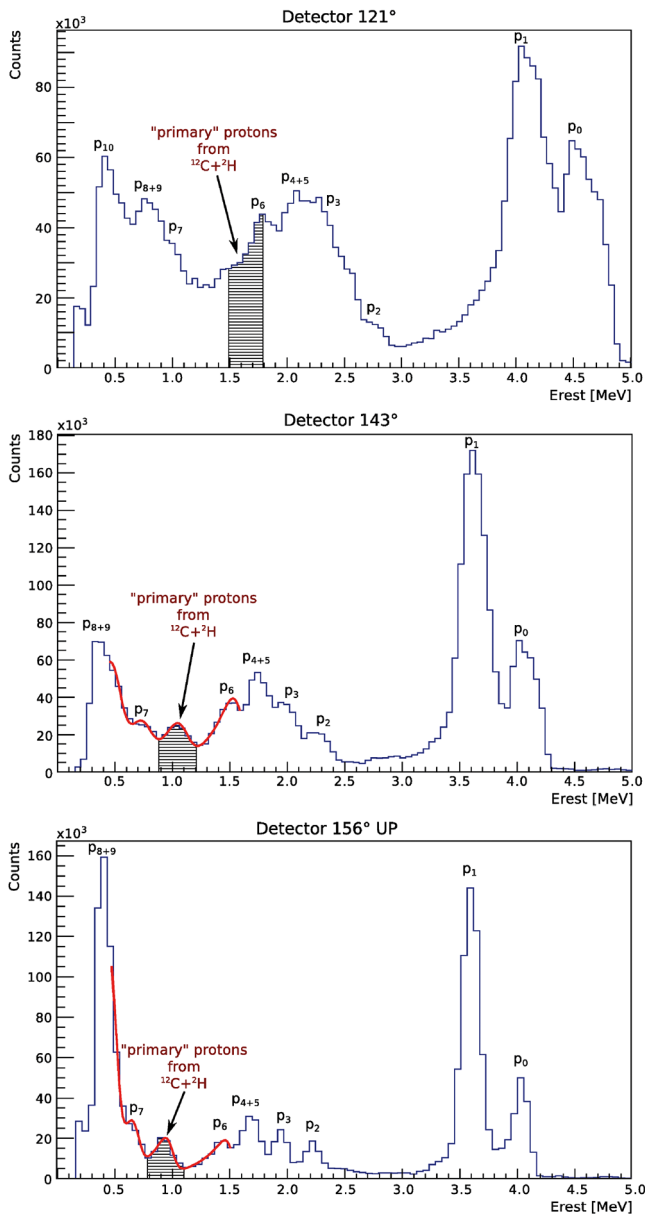
Fig. 5. Sample proton spectra obtained at 8 MeV beam energy, on NG targets and with aquarium. The primary proton peak, arising from the $d(^{12}C, p)^{13}C$ reaction on target deuterium contamination, is marked with an arrow and a hatched area, while other peaks arise from the $^{12}C(^{12}C, p)^{23}Na$ reaction and are labelled according to the excitation state of the residual nucleus.

sphere (aquarium) are shown in fig. 5 for detectors D121, D143, and D156U (top, middle and bottom panel, respectively; D156D data were discarded due an excessively high discrimination threshold that affected the low-energy part of the spectrum thus preventing further analysis). Peaks arising from the $^{12}C(^{12}C, p)^{23}Na$ reaction are labelled according to the excited state of the residual nucleus (p_0 corresponding to transitions leaving ^{23}Na in its ground state, p_1 in its first excited state and so on). The primary proton peak, due to the $d(^{12}C, p)^{13}C$ reaction on deuterium
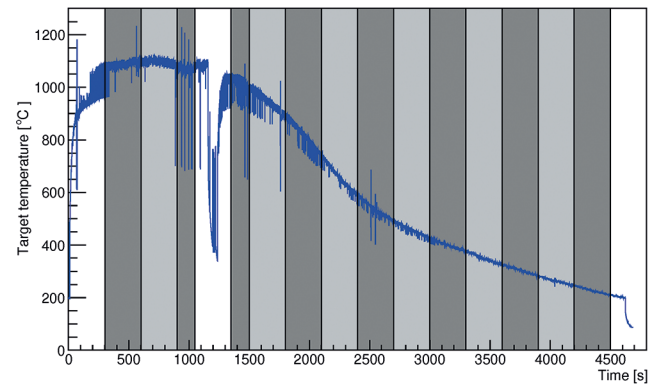
Fig. 6. Time evolution of target temperature (HOPG target) at the beam spot position under $^{12}C^{3+}$ beam bombardment ($E = 8$ MeV, $i = 7$ pμA). The temperature increases to about 1100 °C in 500 seconds. Shaded areas correspond to the time intervals used in the data analysis. Intervals where the temperature shows large fluctuations (*e.g.*, following beam current instabilities) were excluded from the analysis. See text for details.

contamination in the target, is shown as a hatched area which defines the ROI for the present study. Its location for each detector was corroborated by GEANT4 simulations [25]. However, depending on detection angle, contributions to the primary proton peak from nearby peaks vary and must be properly taken into account. In particular, notice that p_6 almost completely overlaps with the ROI in D121, while its contribution to the ROIs is lower in D143 and D156U. On the contrary, p_7 greatly contributes to the ROIs in D143 and D156U. To account for these contributions, four skewed Gaussians were used to fit the low-energy part of the spectrum (see fig. 5). No fit was attempted for the D121 spectrum as it was impossible to disentangle the primary proton peak from p_6 and no further analysis was done.

To assess whether and to what extent the deuterium content in the targets was affected by the target temperature, data were analysed according to the following procedure:

a) Each run was segmented into time intervals (time-divided spectra), typically 300 s each. Intervals where the temperature showed variations greater than 100 °C or an erratic behaviour, *e.g.* due to beam current spikes, were either segmented into shorter time intervals or discarded from further data analysis. As an example, fig. 6 shows the time evolution of the target temperature at the beam spot position obtained during $^{12}C^{3+}$ beam bombardment of an HOPG target, without aquarium, at $E = 8$ MeV and with an average beam current of 7 pμA.

b) For each interval, the deposited charge on target was calculated as the integral of the corresponding beam-current reading during that interval and the corresponding spectrum normalised accordingly.

c) For each interval, background contributions from nearby peaks were subtracted from the ROI of primary protons as discussed in sect. 4.3.

d) The resulting (background-subtracted) primary-proton yield $Y_{\mathrm{p}}(d)$ (counts/C) was then associated to the median temperature of the interval. The temperature uncertainty was calculated using the quantiles technique such that 68% of the distribution is within 1σ [26]. The error on the yield was dominated by the statistical error of the integrated peak and the nominal error (1%) of the charge current integrator. Typical total errors were about 5%.

The procedure was then repeated for all time intervals in a run, and for different runs with and without aquarium on both HOPG and NG targets.

4.3 Background subtraction from nearby peaks

Given that the statistics of each time-divided spectrum were very low, the contribution of the nearby peaks to the primary proton group of the $\mathrm{d}(^{12}\mathrm{C},\mathrm{p})^{13}\mathrm{C}$ reaction was estimated using the full statistics spectra, *i.e.*, not divided into time intervals. Four skewed Gaussian functions were used to simultaneously fit all peaks from p_6 to p_9 including the primary-proton peak, as shown in fig. 5. Parameters from the best fit were then used to calculate the total yield $Y_{\mathrm{fit}}^{\mathrm{full}}$ under the primary protons peak from the full statistic spectrum. A comparison between $Y_{\mathrm{fit}}^{\mathrm{full}}$ and the integral of counts in the whole ROI, $Y_{\mathrm{ROI}}^{\mathrm{full}}$, was finally used to obtain the nearby peaks' contribution to the ROI, $Y_{\mathrm{bkg}}^{\mathrm{full}}$, as

$$Y_{\mathrm{bkg}}^{\mathrm{full}} = Y_{\mathrm{ROI}}^{\mathrm{full}} - Y_{\mathrm{fit}}^{\mathrm{full}}. \tag{1}$$

At this point, it was necessary to establish a procedure that allowed us to scale $Y_{\mathrm{bkg}}^{\mathrm{full}}$ to individual time intervals. This was done by considering that proton peaks from the $^{12}\mathrm{C}(^{12}\mathrm{C},\mathrm{p})^{23}\mathrm{Na}$ reaction scale with charge in the same proportion and, in particular, as p_0 and p_1 peaks, which remain comparatively intense even for low-statistics time-divided spectra. Thus, we defined a scaling factor R as

$$R = \frac{Y_{\mathrm{bkg}}^{\mathrm{full}}}{Y_{(\mathrm{p}_0+\mathrm{p}_1)}^{\mathrm{full}}}, \tag{2}$$

such that, for each time interval normalised in charge, the net (background-subtracted) primary proton yield, $Y_{\mathrm{p}}(d)$ can be obtained as

$$Y_{\mathrm{p}}(d) = Y_{\mathrm{ROI}} - R * Y_{(\mathrm{p}0+\mathrm{p}1)}, \tag{3}$$

with Y_{ROI} being the integral of counts in the ROI of the time-divided spectrum (no fitting procedure was possible because of low statistics). Note that all yields in eq. (3) are properly normalised to charge.

5 Results

The results obtained from the data analysis described in sects. 4.2 and 4.3 are show in fig. 7. Here, the primary proton yields $Y_{\mathrm{p}}(d)$, in counts/C, are taken as a proxy for deuterium content and plotted as a function of target
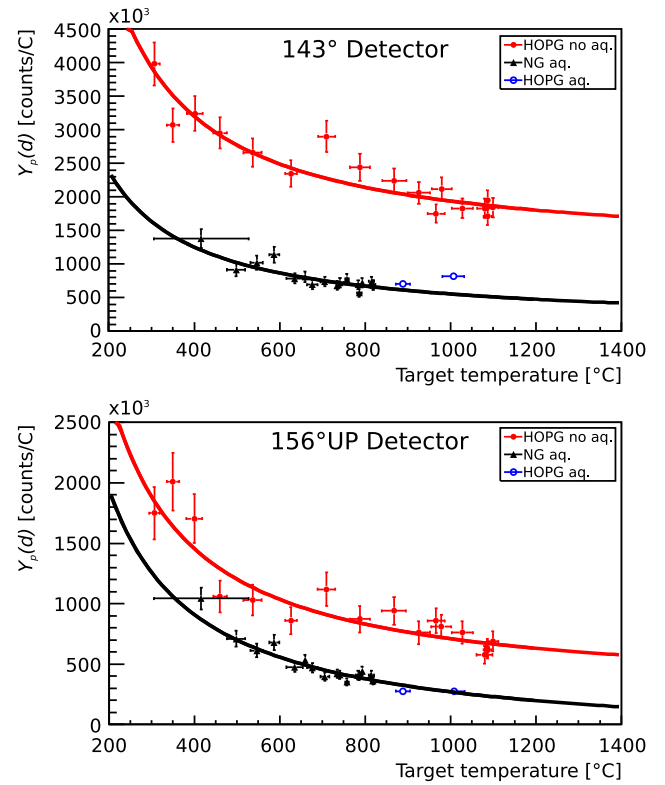
Fig. 7. Deuterium content, as measured by primary proton yields (counts/C), as a function of target temperature, for different detectors and different targets (HOPG, NG), with or without nitrogen aquarium ("aq." and "no aq.", respectively, in the legend). The curves represent best fits to the data.

Table 1. Deuterium reduction (in percentage) observed in each detector over the temperature range $T = 200\text{--}1200\,^{\circ}\mathrm{C}$ for HOPG and NG targets without and with aquarium, respectively (see text for details).

Target	Aquarium	D143	D156U
HOPG	no	$(67 \pm 7)\%$	$(77 \pm 10)\%$
NG	yes	$(80 \pm 8)\%$	$(90 \pm 7)\%$

temperature. The lines through the data sets represent best fits obtained using a power-law function $A \times T^B + C$ (T is the temperature of the target) with fit parameters A, B and C.

All curves in fig. 7 show similar trends: specifically, a reduction in deuterium content is observed with increasing target temperatures from $200\,^{\circ}\mathrm{C}$ to $1200\,^{\circ}\mathrm{C}$ regardless of target and experimental conditions (with or without aquarium). Quantitative values for both detectors and targets are given in table 1, where uncertainties in the deuterium content were estimated by artificially inflating error bars on $Y_{\mathrm{p}}(d)$ until the $\tilde{\chi}^2$ of the fit was about 1. Note, that even though slightly different values are obtained for the same target and different detectors (as a result of the background subtraction), these are in fair agreement with one another within error bars. Likewise, results obtained with the same detector but different targets are also in relatively good agreement.

Note, however, that a comparison between runs on the HOPG target with aquarium (blue open symbols in fig. 7) and without aquarium shows that the deuterium content on target can be further reduced by about a factor of 2.5 at temperatures 900–1000 °C. No runs were obtained at lower temperatures with the HOPG target and aquarium and further conclusions at lower temperatures cannot be drawn in this case. However, these two data points follow the general trend obtained for the NG target with aquarium where the same factor of 2.5 lower deuterium content is obtained compared to the case HOPG target and no aquarium. This result suggests that the presence of the aquarium contributes to a reduction of deuterium content on target by affecting its concentration in the rest gas (see fig. 2).

The results obtained here supersede those reported in [23], where a less accurate procedure for the background subtraction had been adopted.

6 Discussion and conclusions

The results presented in the previous section provide a quantitative trend of the reduction in deuterium contamination in the carbon targets used in this study and demonstrate a correlation with the presence of a nitrogen atmosphere.

In order to have an indication of the deuterium content on the targets, ^{12}C + ^{2}H cross-section values by Kokkoris *et al.* [27] were integrated over a range of deuterium energies $E_{\rm d} = 0$–1.35 MeV and converted into an inferred yield, assuming a uniform deuterium content in the targets and a constant stopping power. To avoid angular distribution effects, only data measured at $155°$ (similar to our detection angles) were considered. The ratio between the inferred yield (based on cross-sections data [27]) and ours was found to be consistent with previous experimental evidence that ^{1}H and ^{2}H contaminations mostly come from the bulk of the targets rather than from their surface (~ 0.3 at-ppm) [28]. However, since the nitrogen aquarium was found to reduce the target contamination, we can conclude that there is a target uptake of light contaminants from the residual gas.

Our results suggest that an improved measurement of the low-energy ^{12}C + ^{12}C cross-sections can be attained already at target temperatures above $400°$C and by enclosing the scattering chamber in a nitrogen atmosphere. A more systematic study of deuterium contaminant reduction would likely require more detailed investigations, which however go beyond the intended purpose of this study.

In summary, we have investigated the change of deuterium contamination in natural graphite and highly ordered pyrolytic graphite targets, upon beam bombardment by intense (up to $50\,\mu$A) ^{12}C^{+3} beams at the Centre for Isotopic Research on the Cultural and Environmental heritage, Caserta (Italy). The content of deuterium on target was assessed by measuring proton yields from the d(^{12}C, p)^{13}C reaction as a function of target temperature.

The target temperature was continuously monitored during beam bombardment with a calibrated thermo-camera and its value recorded concurrently with the beam current on target. The target temperature could be varied in a controlled way by either regulating the water cooling flux on the target ladder and/or by varying the beam current on target. Results indicate reductions in deuterium content up to 70–85% in both types of targets over a temperature range $T = 200$–$1200°$C. A further reduction by a factor of about 2.5 in absolute value was observed when enclosing the scattering chamber in a nitrogen atmosphere, which acts to minimise ^{1,2}H uptake from the residual gas of the chamber.

To our knowledge, this study represents the first attempt at a quantitative assessment of deuterium contamination in carbon targets under intense carbon-beam bombardment.

Results from our investigation of the ^{12}C(^{12}C, p)^{23}Na and ^{12}C(^{12}C, α)^{20}Ne reactions will be presented in forthcoming publications.

References

1. A. Chieffi *et al.*, Astrophys. J. **502**, 737 (1998).
2. El Eid *et al.*, Astrophys. J. **611**, 452 (2004).
3. J. Patterson, H. Winkler, C. Zaidins, Astrophys. J. **157**, 367 (1969).
4. M. Mazarakis, W. Stephens, Phys. Rev. C **7**, 4 (1973).
5. H.W. Becker, K.U. Kettner, C. Rolfs, H.-P. Trautvetter, Z. Phys. A **312**, 305 (1981).
6. M. High, B. Ĉujec, Nucl. Phys. A **282**, 181 (1977).
7. K.U. Kettner *et al.*, Z. Phys. A **75**, 65 (1980).
8. P. Rosales, E. Aguilera, Rev. Mexi. Fís. **49**, 88 (2003).
9. L. Barrón-Palos, E. Chavez, Rev. Mexi. Fís. **50**, 18 (2004).
10. L. Barrón-Palos *et al.*, Eur. Phys. J. A **25**, 645 (2005).
11. L. Barrón-Palos *et al.*, Nucl. Phys. A **779**, 318 (2006).
12. E. Aguilera *et al.*, Phys. Rev. C **73**, 064601 (2006).
13. T. Spillane *et al.*, Phys. Rev. Lett. **98**, 122501 (2007).
14. C.L. Jiang *et al.*, Nucl. Instrum. Methods Phys. Res. A **682**, 12 (2012).
15. C.L. Jiang *et al.*, Phys. Rev. C **97**, 012801 (2018).
16. M. Wiescher, Annu. Rev. Astron. Astrophys. **50**, 165 (2012).
17. X.D. Tang *et al.*, Nucl. Phys. Astrophys. V **337**, 012016 (2012).

18. A. Zaloznik *et al.*, Nucl. Instrum. Methods Phys. Res. B **371**, 167 (2016).

19. F. Terrasi *et al.*, Nucl. Instrum. Methods B **259**, 14 (2007).

20. `https://www.instrumart.com/assets/Flir-SC325-Datasheet.pdf`.

21. M. Romoli *et al.*, Eur. Phys. J. A (2018) `https://doi.org/10.1140/epja/i2018-12575-5`.

22. `http://www.canberra.com` (last accessed: July 4, 2018).

23. L. Morales-Gallegos, *Carbon burning in stars: An experimental study of the* $^{12}C(^{12}C,p)^{23}Na$ *reaction towards astrophysical energies*, PhD Thesis, The University of Edinburgh (2017).

24. J. Zickefoose, ^{12}C+^{12}C *fusion: Measurement and advances toward the Gamow energy*, PhD Thesis, University of Connecticut, US (2010).

25. L. Zhang, *Simulations of deuterium contamination for* ^{12}C $+$ ^{12}C *reaction studies*, internal report, The University of Edinburgh (2017).

26. P.R. Bevington, *Data Reduction and Error Analysis for the Physical Sciences* (McGraw-Hill, 2003).

27. M. Kokkoris *et al.*, Nucl. Instrum. Methods Phys. Res. B **249**, 77 (2006).

28. P. Reichart *et al.*, Nucl. Instrum. Methods Phys. Res. B **249**, 286 (2006).